Journal of Physics: Conference Series **544** (2014) 012012 doi:10.1088/1742-6596/544/1/012012

Large scale reconstruction of the solar coronal magnetic field

T. Amari[1], J.-J. Aly[2], P. Chopin [1], A. Canou[1], & Z. Mikic[3]

[1]CNRS, Centre de Physique Théorique de l'Ecole Polytechnique, F-91128 Palaiseau Cedex, France

[2]AIM - Unité Mixte de Recherche CEA - CNRS - Université Paris VII - UMR n^0 7158, Centre d'Études de Saclay, F-91191 Gif sur Yvette Cedex, France

[3]Predictive Science Inc., San Diego, CA 92121, USA

E-mail: amari@cpht.polytechnique.fr

Abstract. It is now becoming necessary to access the global magnetic structure of the solar low corona at a large scale in order to understand its physics and more particularly the conditions of energization of the magnetic fields and the multiple connections between distant active regions (ARs) which may trigger eruptive events in an almost coordinated way. Various vector magnetographs, either on board spacecraft or ground-based, currently allow to obtain vector synoptic maps, composite magnetograms made of multiple interactive ARs, and full disk magnetograms. We present a method recently developed for reconstructing the global solar coronal magnetic field as a nonlinear force-free magnetic field in spherical geometry, generalizing our previous results in Cartesian geometry. This method is implemented in the new code XTRAPOLS, which thus appears as an extension of our active region scale code XTRAPOL. We apply our method by performing a reconstruction at a specific time for which we dispose of a set of composite data constituted of a vector magnetogram provided by SDO/HMI, embedded in a larger full disk vector magnetogram provided by the same instrument, finally embedded in a synoptic map provided by SOLIS. It turns out to be possible to access the large scale structure of the corona and its energetic contents, and also the AR scale, at which we recover the presence of a twisted flux rope in equilibrium.

1. Introduction

The problem of the reconstruction of the solar coronal magnetic field from photospheric boundary data has been a very active topic of research in recent years due to the arrival of high resolution and low noise vector magnetographs either on the ground, such as THEMIS and SOLIS, or on board present solar missions, such as HINODE and SDO/HMI, and future ones, such as EST and SOLAR-ORBITER. We refer the reader to Aly & Amari (2007) and Wiegelmann & Sakurai (2012) for a review of all existing reconstruction methods. We just recall here for the purpose of this Paper that the main methods proposed so far are the optimisation methods (Wiegelmann, 2004), which use all photospheric data and try to minimize a cost function measuring the difference between the computed transverse field and the measured one, the magnetohydrodynamic relaxation methods (Valori *et al.*, 2005), and the Grad-Rubin methods (Sakurai, 1981; Amari *et al.*, 1999; Inhester & Wiegelmann, 2006; Wheatland, 2007). Recently Amari *et al.* (2006) presented two methods that attempt to solve the Grad-Rubin Boundary

Value Problem (BVP), namely XTRAPOL and FEMQ, the former based on a finite difference approximation and the latter on a finite element approximation.

Most of these methods have addressed the active region (AR) scale and have thus used the Cartesian geometry framework in which Sun's curvature is neglected. Such an approximation, however, becomes invalid when one attempts to understand the large scale coronal structures and their dynamics (Mackay & Yeates, 2012). With the arrival of SOLIS and SDO/HMI, it is possible to obtain composite high resolution vector magnetograms made of several active regions, or embedded in a full disk vector magnetogram and/or synoptic vector magnetograms. Furthermore vector magnetic fields are also measured on the whole surface of many stars with different techniques, although at a lower resolution and with less accuracy (Donati *et al.*, 2007).

This raises the issue of building up reconstruction models at global scale. Extension of the Cartesian models to spherical ones has thus recently become an important question, and actually such an extension has already been done in the optimization methods settings (Wiegelmann, 2007). It must be noted that, either for full disk or for synoptic maps, strong constraints on spatial resolution are imposed due to the fact that ARs represent only a small fraction of the Sun's surface. Therefore neither uniform nor non-uniform structured meshes can fit such structures in an optimal way.

In the present Paper, we present a new code, XTRAPOLS, that allows the reconstruction of the nonlinear force-free field in the exterior of a spherical region. This code is based on the iterative Grad-Rubin scheme that we have already implemented in Cartesian geometry (Amari *et al.*, 2006) and is now implemented in spherical coordinates. We favor this approach because it corresponds to a well-posed BVP. Moreover it has already proved to be quite efficient in the previously considered Cartesian context, and has allowed us to obtain significant quantitative results when applied to observational data (Bleybel *et al.*, 2002; Régnier *et al.*, 2002; Régnier & Amari, 2004; Régnier *et al.*, 2005; DeRosa *et al.*, 2009; Canou *et al.*, 2009; Canou & Amari, 2010; Petrie *et al.*, 2011).

XTRAPOLS is a massively parallel code, and as such it is able to handle the large amounts of data currently provided by vector magnetographs, with fields being measured on a very large scale and with a very high resolution. We apply this code to the reconstruction of the global coronal field at some particular date, using as boundary conditions a composite data set obtained by using vector magnetograms provided by SDO/HMI at both the AR scale and the full disk scale, and a SOLIS synoptic map on the rest of the Sun. We show that the model allows to determine both the large scale structure of the corona and the small scale structure of an AR. In particular, we find the presence of a twisted flux rope in equilibrium, which can possibly be responsible for the energization of the AR and the subsequent occurrence of a large scale eruptive event. More details on the computational method and the testing of the code can be found in Amari *et al.* (2013)., which was submitted for publication after the ICMS Workshop.

2. Method

2.1. The continuous BVP

In the theoretical model we consider, the corona and the photosphere are represented by a domain Ω that is the exterior of a sphere rather than the half-space $D = \{z > 0\}$ considered previously. This model thus differs from the previously developed Ω is assumed to be filled up with a low beta plasma embedded in a magnetic field $\mathbf{B}$ that is taken to be force-free and to decrease sufficiently fast to zero at infinity. Therefore, it does obey the equations

$$\boldsymbol{\nabla} \times \mathbf{B} = \alpha \mathbf{B}\,, \tag{1}$$

$$\boldsymbol{\nabla} \cdot \mathbf{B} = 0\,. \tag{2}$$

It results at once from Eqs. (1)-(2) that the function α satisfies the constraint

$$\mathbf{B} \cdot \boldsymbol{\nabla}\alpha = 0\,, \tag{3}$$

which merely states that α keeps a constant value along any field line.

The set of equations (1)-(3) has a mixed elliptic-hyperbolic structure. Basically, it can be decomposed into an elliptic part for $\mathbf{B}$ (Eqs. (1)-(2) with α given), and an hyperbolic part for α (Eq. (3) with $\mathbf{B}$ given). To solve for the elliptic part, one should give the normal component B_n of the magnetic field on $\partial\Omega$, while to solve for the hyperbolic one, Eq. (3) indicates that the value of α should be given on the part $\partial\Omega^+$ of $\partial\Omega$ where $B_n > 0$, say. This leads us to consider the BVP first introduced by Grad & Rubin (1958). It consists of Eqs. (1)-(3) along with the boundary conditions

$$B_n|_{\partial\Omega} = b_0\,, \tag{4}$$
$$\alpha|_{\partial\Omega^+} = \alpha_0\,, \tag{5}$$

where b_0 and α_0 are two given regular functions, and the asymptotic condition

$$\lim_{|\mathbf{r}|\to\infty} |\mathbf{B}| = 0\,. \tag{6}$$

In the numerical practice we consider the bounded domain $\Omega_b = \{r_0 < r < r_1\}$, limited by the spherical surfaces $S_0 = \{r = r_0\}$ (the photosphere) and $S_1 = \{r = r_1\}$, instead of the unbounded domain Ω. Then the asymptotic condition (6) is no longer relevant and the boundary conditions (4)-(5) are imposed on the whole $\partial\Omega_b$.

2.2. Principle of the Iterative Grad-Rubin method

In the Grad-Rubin method, the BVP above is solved iteratively, with its elliptic and hyperbolic parts being considered in turn at each step. More precisely, we look for a sequence $(\mathbf{B}^{(n)}, \alpha^{(n)})$ solution of

$$\mathbf{B}^{(n)}.\nabla\alpha^{(n)} = 0 \quad \text{in} \quad \Omega_b\,, \tag{7}$$
$$\alpha^{(n)}|_{\partial\Omega_b^+} = \alpha_0\,, \tag{8}$$

and

$$\nabla\times\mathbf{B}^{(n+1)} = \alpha^{(n)}\mathbf{B}^{(n)} \quad \text{in} \quad \Omega_b\,, \tag{9}$$
$$\nabla\cdot\mathbf{B}^{(n+1)} = 0 \quad \text{in} \quad \Omega_b\,, \tag{10}$$
$$B_r^{(n+1)}|_{\partial\Omega_b} = b_0\,. \tag{11}$$

The iteration process is initialized by choosing for $\mathbf{B}^{(0)}$ the potential field with the normal component b_0, i.e., the unique solution of

$$\nabla\times\mathbf{B}^{(0)} = 0 \quad \text{in} \quad \Omega_b, \tag{12}$$
$$B_r^{(0)}|_{\partial\Omega_b} = b_0\,. \tag{13}$$

A fundamental property of our method is that it is well-posed – in particular it is stable with respect to changes in the boundary conditions. This makes a major difference with the methods, recalled above, that use the three components of the photospheric field as boundary conditions: as there is most generally no exact force-free solutions matching such conditions, these methods have to deal with ill-posedness. Another point is worth noticing. In the Grad-Rubin BVP one fixes the values of α in only one polarity. The values of α in the other polarity are obtained by computing the solution, and do not match the observed values α_0. Then reversing the role of the two polarities leads to a different solution. A unique solution for which the computed

α is as close as possible to the observed α_0 on the whole S can however be obtained by using the recently proposed Grad-Rubin-Optimization-Method (Amari & Aly, 2010). The idea is to impose, at each iteration step, the value of α on a line to be a weighted average of the values of α_0 at its two footprints. This new approach has been shown to give good and robust results, but we shall not use it here.

The previous scheme is implemented in spherical coordinates, using a numerical method which is able to run on massively parallel computers. This is required if we want to deal in an efficient way with the large amount of data provided by the observations.

To address the $\nabla \cdot \mathbf{B} = 0$ constraint, XTRAPOLS introduces a vector potential $\mathbf{A}^{(n)}$ and ensures that the iterated numerical field $\mathbf{B}^{(n)} = \nabla \times \mathbf{A}^{(n)}$. To determine $\mathbf{A}^{(n)}$ in a unique way, we impose the gauge conditions

$$\nabla \cdot \mathbf{A}^{(n)} = 0 \quad \text{in } \Omega_b, \tag{14}$$

$$\mathbf{A}_t^{(n)} = \mathbf{A}_{\pi t} \quad \text{on } \partial\Omega_b, \tag{15}$$

where $\mathbf{X}_t$ denotes the component of $\mathbf{X}$ tangent to the boundary and $\mathbf{A}_\pi$ is a specific vector potential of the current-free field $\mathbf{B}_\pi$, i.e.,

$$\mathbf{B}_\pi = \nabla \times \mathbf{A}_\pi. \tag{16}$$

$\mathbf{A}_\pi$ is required to satisfy the gauge conditions

$$A_{\pi r}(r, \theta, \varphi) = 0, \tag{17}$$

$$\nabla \cdot \mathbf{A}_\pi(r_0, \theta, \varphi) = 0, \tag{18}$$

which implies that $\nabla \cdot \mathbf{A}_\pi = 0 \quad$ in Ω_b. To compute $\mathbf{A}_\pi$ on the boundary: (i) We introduce a scalar potential $\chi_\pi(r, \theta, \varphi)$ such that $\mathbf{A}_\pi = \nabla\chi_\pi \times \hat{\mathbf{r}} \quad$ in Ω_b. (ii) We impose $\chi(r_0, \theta, \varphi)$ to be the unique solution with zero average value of the equation $-\nabla_\perp^2 \chi = B_r$ on S_0. Solving this equation determines $\mathbf{A}_\pi$ on S_0. (iii) We introduce the standard representation $\mathbf{B}_\pi = \nabla\psi_\pi$, and compute the scalar potential ψ_π by solving Laplace equation $-\nabla^2\psi_\pi = 0$ in Ω_b along with the boundary condition $\partial_r\psi_\pi = B_r$ on $S_0 \cup S_1$. (iv) χ_π is thus given by

$$\chi_\pi(r, \theta, \varphi) = \chi_\pi(r_0, \theta, \varphi) + \int_{r_0}^{r} \psi_\pi(r', \theta, \varphi)\, \mathrm{d}r', \tag{19}$$

from which we get $\mathbf{A}_\pi$ on S_1.

In our vector potential formulation, α is determined by solving

$$\nabla \times \mathbf{A}^{(n)} . \nabla\alpha^{(n)} = 0 \quad \text{in} \quad \Omega_b\,, \tag{20}$$

$$\alpha^{(n)}|_{\partial\Omega_b^+} = \alpha_0\,, \tag{21}$$

which is just a rewriting of Eqs. (7)-(8). The boundary value of α is thus directly imposed at each iterative step, rather than being progressively increased to its nominal value through a second iterative loop as was done in Amari *et al.* (1999). In other words, we keep only the inner Grad-Rubin iteration loop in the two-level iteration procedure used in the latter paper.

Eqs. (20)-(21) are solved by the method of characteristics. The characteristic $\mathbf{X}(s, \mathbf{r})$ passing through the point $\mathbf{r} \in \Omega_b$ is a solution of (Amari *et al.*, 1999, 2006)

$$\mathbf{X}' = \mathbf{B}(\mathbf{X})\,, \tag{22}$$

$$\mathbf{X}(0) = \mathbf{r}\,, \tag{23}$$

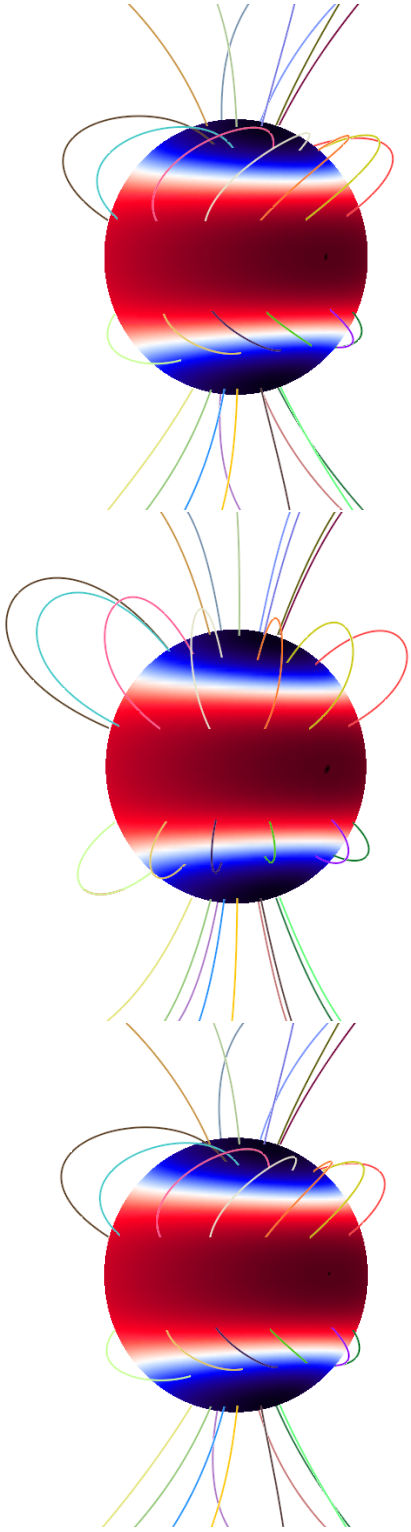

Figure 1. Reconstruction of the test field. We have drawn a set of field lines of the exact Low-Lou solution (top), one of the potential (current-free) field (middle), and one of the solution computed with our algorithm with a resolution of $80 \times 160 \times 320$ (bottom).

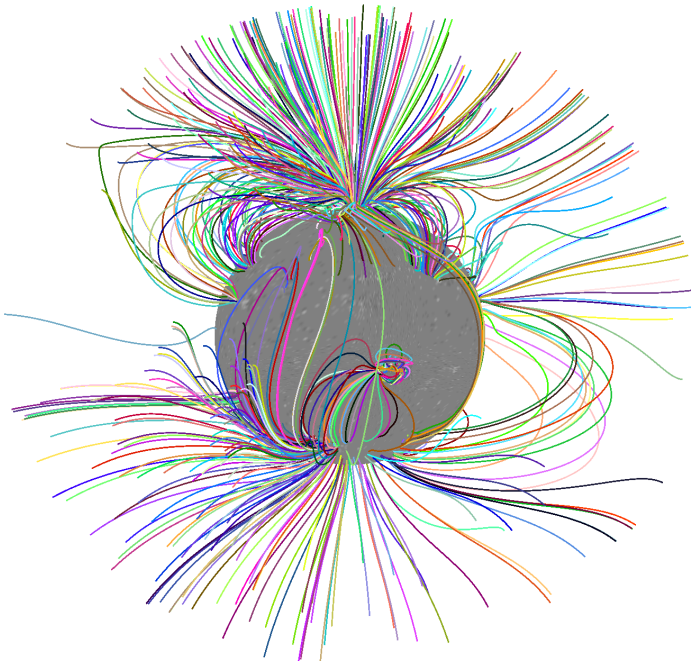

Figure 2. Set of field lines of the reconstructed global solar force-free magnetic field. The calculation is done with resolution $171 \times 251 \times 363$ and use AR scale and full disk magnetograms from SDO/HMI, and synoptic map from SOLIS.

where the prime symbol stands for differentiation with respect to the parameter s running along that curve. Then for any node $\mathbf{r}_h \in \Omega_b$ at which α is defined, one gets α_h as

$$\alpha(\mathbf{r}_h) = \alpha_0(\mathbf{X}^+(\mathbf{r}_h)) \,, \tag{24}$$

where $\mathbf{X}^+(\mathbf{r}_h)$ is the intersection of $\{\mathbf{X}(\mathbf{r}; s) : s < 0\}$ with $\partial\Omega_b^+$. Since α_0 is known at nodes that do not in general coincide with $\mathbf{X}^+(\mathbf{r}_h)$, we use an interpolation from their four nearest neighbors.

We define the location of α on the cell vertices. We use either a high order Adams-Bashforth integration scheme with adaptive step size or a 4th order Runge Kutta scheme, which also allows us to capture accurately the ending point of the characteristics defining the limits of the computational box. As already discussed in Cartesian geometry (Amari & Aly, 2010), it is possible to have at the k-th iteration of the scheme some field lines that do not intersect the part of the photospheric boundary where $B_r > 0$ but emerge from the upper boundary. In that case we set

$$\alpha^{(k)}(\mathbf{r}) = \alpha_0(\mathbf{X}^-(\mathbf{r})). \tag{25}$$

Our convergence criterion for the sequence of fields $\mathbf{B}^{(n)}$ is chosen to be

$$\frac{|| \mathbf{B}^{(n+1)} - \mathbf{B}^{(n)} ||_{L^2(\Omega_b)}}{|| \mathbf{B}^{(n)} ||_{L^2(\Omega_b)}} \quad < \quad \epsilon \,, \tag{26}$$

with $\epsilon = 10^{-6}$. We found that a total number of iterations of about $30-50$ is sufficient to achieve convergence in most cases, and the stopping criteria is robust with respect to changes in the data put as boundary conditions. Compared to the Cartesian version, to solve the hyperbolic

problem we need to use at a given point in the domain a mapping from spherical to Cartesian coordinates while going back along a characteristic. The algorithm presented is parallel for both the Elliptic and the Hyperbolic problems (only with one global field for the latter). We use domain decomposition with the MPI interface on our staggered mesh.

3. Application to a semi analytic case

We have applied successfully our solver to the reconstruction of the nonlinear force-free Low-Lou solution (Low & Lou, 1990). In an auxiliary spherical coordinate system (r', θ', φ') centered at O', this axisymmetric field has the representation

$$\mathbf{B} = \nabla A \times \frac{\hat{\varphi}'}{r' \sin\theta'} + F \frac{\hat{\varphi}'}{r' \sin\theta'}, \tag{27}$$

with the poloidal flux function $A(r', \theta')$ and current function $F(r', \theta')$ being given by, respectively,

$$A(r', \theta') = \frac{P(\mu')}{(r')^n}, \tag{28}$$

$$F(r', \theta') = aA^{1+1/n} = a\frac{P^{1+1/n}(\mu')}{(r')^{n+1}}. \tag{29}$$

Here $\mu' = \cos\theta'$, and P is a solution of a nonlinear ordinary differential equation satisfying $P(\pm 1) = 0$.

For testing our numerical procedure with an asymmetric field depending on the three coordinates r, θ, φ, we introduce the solution having the quadrupolar structure and the "stretching parameter" $n = 1$ into our model by imposing its axis of symmetry $O'z'$ to coincide with the axis Oz of our main frame, with the center O' being located at the position $\overrightarrow{OO'} = d\hat{\mathbf{z}}$. We take for d the value selected by Wiegelmann (2007), who has already used this shifting procedure, thus making it possible to compare his results with ours.

Table 1 shows some of the diagnostics, often called figures of merit, already used for Cartesian coordinates calculations in Amari *et al.* (1999, 2006) and in Schrijver *et al.* (2006), to which we refer for precise definitions. The various quantities are evaluated for $\mathbf{u}$ equal to the exact solution and $\mathbf{v}$ equal to the numerical solution obtained with XTRAPOLS. They have to be compared with the reference values $VC(\mathbf{u}, \mathbf{u}) = CS(\mathbf{u}, \mathbf{u}) = 1$, $NVE(\mathbf{u}, \mathbf{u}) = MVE(\mathbf{u}, \mathbf{u}) = 0$, $\epsilon_M = 1$. We also found important to report estimates of $\nabla \cdot \mathbf{B}$, as well as the CPU time, both figures providing additional measures of the quality of the solution.

Table 1. Various error diagnostics allowing to evaluate the quality of the test field reconstructions performed with XTRAPOLS for three numerical resolutions:

RESOLUTION	VC	CS	NVE	MVE	ϵ_M	$\|\| \text{div}\mathbf{B} \|\|_{L^\infty}$	Time
$20 \times 40 \times 80$	0.9972	0.9980	0.0696	0.0783	1.008	1.53510^{-13}	61s
$40 \times 80 \times 160$	0.9983	0.9985	0.0650	0.0610	1.002	$1.278\ 10^{-12}$	800s
$80 \times 160 \times 320$	0.9992	0.9993	0.0612	0.0587	1.001	1.18410^{-12}	10077s

As shown on Fig. 1 the field lines of the numerically computed nonlinear force-free configuration are very similar to those of the exact solution. Note that they are quite far from those of the potential (current-free) field.

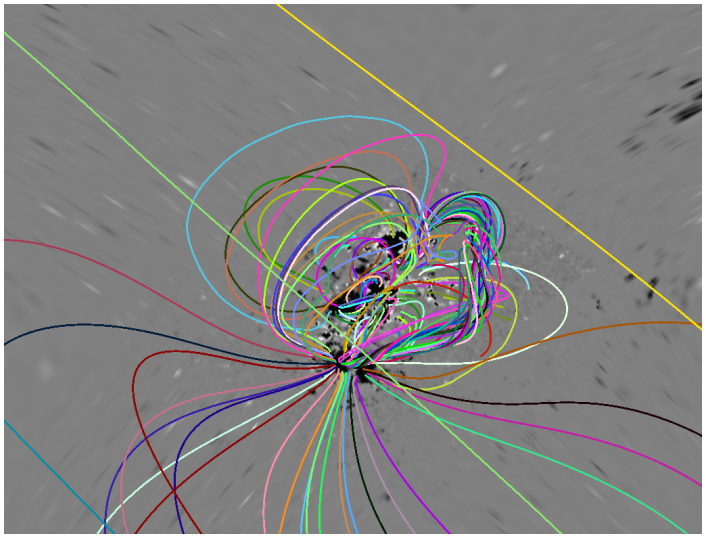

Figure 3. Structure at AR scale of the global solution shown in Figure 1. A twisted flux rope in equilibrium is neatly seen to be present.

4. Application to a composite magnetogram (SDO/HMI-SOLIS)

We have applied our method to the determination of the full Sun coronal magnetic configuration of February 14, 2011, 22:00 UT, using a composite magnetogram provided by two instruments. We give here only a preliminary account of our results, which are explained in details in a forthcoming paper.

During the first half of February 2011, the disk was characterized by the presence of the AR 11158, which was the sit of a very strong eruptive activity involving a CME and an X-class flare on February 15 at 01:40 UT. For our reconstruction with XTRAPOLS, we use as boundary conditions a vector magnetogram provided by SDO/HMI, embedded in a larger full disk vector magnetogram provided by the same instrument, finally embedded in a synoptic map provided by SOLIS. We also used a special processing, and set the current to zero but in the vicinity of AR 11158, where the accuracy of our mesh was high enough to take it into account. The calculations are done with a numerical resolution of 120x200x340 in spherical coordinates.

The solution allows us to catch the large scale magnetic structure (see Fig. 2), as well as the smaller AR scale (see Fig. 3). The structure of the AR can be very precisely characterized and one may note the presence of a twisted flux rope in equilibrium. This rope is possibly responsible for the energization of the AR and it may have stored the large amount of free magnetic energy that was later the source of the large scale eruptive event.

Acknowledgments

We are grateful to the referee for his careful reading of the paper. We thank the Centre National d'Etudes Spatiales (CNES) for support.

References

Aly, J.-J. & Amari, T. 2007 Structure and evolution of the solar coronal magnetic field. *Geophys. Astrophys. Fluid Dyn.* **101**, 249–287.

Amari, T. & Aly, J.-J. 2010 Observational constraints on well-posed reconstruction methods and the optimization-Grad-Rubin method. *Astron. Astrophys.* **522**, A52.

Amari, T., Aly, J.J., Canou, A. & Mikic, Z. 2014 Reconstruction of the solar coronal magnetic field in spherical geometry. *Astron. Astrophys.* **553**, A43-A49.

Amari, T., Boulmezaoud, T. Z. & Aly, J.-J. 2006 Well posed reconstruction of the solar coronal magnetic field. *Astron. Astrophys.* **446**, 691-705.

Amari, T., Boulmezaoud, T. Z. & Mikic, Z. 1999 An iterative method for the reconstruction of the solar coronal magnetic field. I. Method for regular solutions. *Astron. Astrophys.* **350**, 1051-1059.

Bleybel, A., Amari, T., van Driel-Gesztelyi, L. & Leka, K. D. 2002 Global budget for an eruptive active region. I. Equilibrium reconstruction approach. *Astron. Astrophys.* **395**, 685–695.

Canou, A. & Amari, T. 2010 A twisted flux rope as the magnetic structure of a filament in active region 10953 observed by Hinode. *Astrophys. J.* **715**, 1566–1574.

Canou, A., Amari, T., Bommier, V., Schmieder, B., Aulanier, G. & Li, H. 2009 Evidence for a pre-eruptive twisted flux rope using the Themis vector magnetograph. *Astrophys. J.* **693**, L27–L30.

DeRosa, M. L., Schrijver, C. J., Barnes, G., Leka, K. D., Lites, B. W., Aschwanden, M. J., Amari, T., Canou, A., McTiernan, J. M., Régnier, S., Thalmann, J. K., Valori, G., Wheatland, M. S., Wiegelmann, T., Cheung, M. C. M., Conlon, P. A., Fuhrmann, M., Inhester, B. & Tadesse, T. 2009 A critical assessment of nonlinear force-free field modeling of the solar corona for active region 10953. *Astrophys. J.* **696**, 1780–1791.

Donati, J.-F., Jardine, M. M., Gregory, S. G., Petit, P., Bouvier, J., Dougados, C., Ménard, F., Collier Cameron, A., Harries, T. J., Jeffers, S. V. & Paletou, F. 2007 Magnetic fields and accretion flows on the classical T Tauri star V2129 Oph. *Mon. Not. R. Astron. Soc.* **380**, 1297–1312.

Grad, H. & Rubin, H. 1958 Hydromagnetic equilibria and force-free fields. In *Proc. 2nd Intern. Conf. on Peaceful Uses of Atomic Energy*, vol. 31, pp. 190–197. United Nations, Geneva.

Inhester, B. & Wiegelmann, T. 2006 Nonlinear force-free magnetic field extrapolations: Comparison of the Grad Rubin and Wheatland Sturrock Roumeliotis algorithm. *Solar Phys.* **235**, 201-221.

Low, B. C. & Lou, Y. Q. 1990 Modeling solar force-free magnetic fields. *Astrophys. J.* **352**, 343–352.

Mackay, D. & Yeates, A. 2012 The Sun's global photospheric and coronal magnetic fields: observations and models. *Living Rev. Solar Phys.* **9** (6).

Petrie, G. J. D., Canou, A. & Amari, T. 2011 Nonlinear force-free and potential-field models of active-region and global coronal fields during the whole heliosphere interval. *Solar Phys.* **274**, 163–194.

Régnier, S. & Amari, T. 2004 3D magnetic configuration of the Hα filament and X-ray sigmoid in NOAA AR 8151. *Astron. Astrophys.* **425**, 345-352.

Régnier, S., Amari, T. & Kersalé, E. 2002 3D Coronal magnetic field from vector magnetograms: non-constant-alpha force-free configuration of the active region NOAA 8151. *Astron. Astrophys.* **392**, 1119-1127.

Régnier, S., Amari, T. & Canfield, R. C. 2005 Self and mutual magnetic helicities in coronal magnetic configurations. *Astron. Astrophys.* **442**, 345–349.

Sakurai, T. 1981 Calculation of force-free magnetic field with non-constant-alpha. *Solar Phys.* **69**, 343-359.

Schrijver, C. J., DeRosa, M. L., Metcalf, T. R., Liu, Y., McTiernan, J., Régnier, S., Valori, G., Wheatland, M. S. & Wiegelmann, T. 2006 Nonlinear force-free modeling of coronal magnetic fields. Part I: A quantitative comparison of methods. *Solar Phys.* **235**, 161-190.

Valori, G., Kliem, B. & Keppens, R. 2005 Extrapolation of a non linear force-free field containing a highly twisted magnetic loop. *Astron. Astrophys.* **433**, 335-347.

Wheatland, M. 2007 Calculating and testing nonlinear force-free fields. *Solar Phys.* **245**, 251-262.

Wiegelmann, T. 2004 Optimization code with weighting function for the reconstruction of coronal magnetic fields. *Solar Phys.* **219**, 87-108.

Wiegelmann, T. 2007 Computing nonlinear force-free coronal magnetic fields in spherical geometry. *Solar Phys.* **240**, 227–239.

Wiegelmann, T. & Sakurai, T. 2012 Solar force-free magnetic fields. *Living Rev. Solar Phys.* **9** (5).